

## Time reverse location of seismic long-period events recorded on Mt Etna

G. S. O'Brien,<sup>1</sup> I. Lokmer,<sup>1</sup> L. De Barros,<sup>1</sup> C. J. Bean,<sup>1</sup> G. Saccorotti,<sup>2</sup> J.-P. Metaxian<sup>3</sup> and D. Patane<sup>4</sup>

<sup>1</sup>*School of Geological Sciences, University College Dublin, Dublin, Ireland. E-mail: gareth.obrien@ucd.ie*

<sup>2</sup>*Sezione di Pisa, Istituto Nazionale di Geofisica e Vulcanologia, Pisa, Italy*

<sup>3</sup>*LGIT, Université de Savoie, IRD, CNRS, Chambéry, France*

<sup>4</sup>*Sezione di Catania, Istituto Nazionale di Geofisica e Vulcanologia, Catania, Italy*

Accepted 2010 October 14. Received 2010 October 14; in original form 2010 June 22

### SUMMARY

We present the first application of a time reverse location method in a volcanic setting, for a family of long-period (LP) events recorded on Mt Etna. Results are compared with locations determined using a full moment tensor grid search inversion and cross-correlation method. From 2008 June 18 to July 3, 50 broad-band seismic stations were deployed on Mt Etna, Italy, in close proximity to the summit. Two families of LP events were detected with dominant spectral peaks around 0.9 Hz. The large number of stations close to the summit allowed us to locate all events in both families using a time reversal location method. The method involves taking the seismic signal, reversing it in time, and using it as a seismic source in a numerical seismic wave simulator where the reversed signals propagate through the numerical model, interfere constructively and destructively, and focus on the original source location. The source location is the computational cell with the largest displacement magnitude at the time of maximum energy current density inside the grid. Before we located the two LP families we first applied the method to two synthetic data sets and found a good fit between the time reverse location and true synthetic location for a known velocity model. The time reverse location results of the two families show a shallow seismic region close to the summit in agreement with the locations using a moment tensor full waveform inversion method and a cross-correlation location method.

**Key words:** Volcano seismology; Computational seismology; Wave propagation.

### 1 INTRODUCTION

Source location of seismic events with emergent arrivals/signals recorded on volcanoes, namely long-period (LP) and tremor, presents a challenging task. These signals have been directly related to magma movement or magma ascent [see Chouet (2003) and McNutt (2005) for reviews of volcano seismology]. Therefore, source location of these events is of fundamental importance to better understand the volcanic plumbing system. The difficulty in locating these events arises in volcanic settings because near-field effects in the seismic wavefield often cannot be ignored since the wavelengths can be large relative to the source–receiver distance and hence the *P*-wave, *S*-wave and surface wave phases can be intertwined. Separate wave phases may not be distinguishable and the wavefield can be significantly distorted by the complex topography and volcanic stratigraphy. Also, the source mechanism is generally poorly understood and poorly constrained restricting the use of location methods based on known source mechanisms. These factors make it extremely difficult to locate LP sources with classic hypocentre determination methods. Alternative methods have been

used, such as particle motion analysis where the ground deformation vector is reconstructed from the three-component seismogram, array techniques where the slowness vector is estimated, (Almendros *et al.* 2001; Métaxian and Lesage 2002; Di Lieto *et al.* 2007), and estimation of the epicentre location based on the amplitude decay of surface or body waves (Battaglia & Aki 2003; Kumagai *et al.* 2010). Waveform inversion to quantify the source mechanism (Ohminato *et al.* 1998; Nakano and Kumagai 2005; Lokmer *et al.* 2007) has also been used to locate LP events but can show a strong trade-off between mechanism and location. These methods use the whole or partial seismic waveform, not only arrival times. More recently, De Barros *et al.* (2009) used a cross-correlation method to locate two distinct families of LP events on Mt Etna. The accuracy of all of these location methods depends on the reliability of the velocity model and on the approximations underlying the different methods, for example, isotropic source, plane wave approximation or a far-field assumption.

In this paper we use a time reverse mirror to locate LP events recorded on Mt Etna. The method can theoretically give information on both the location and mechanism, however, the mechanism

is very sensitive to the velocity model and station distribution and its interpretation can be ambiguous. Time reversal involves taking LP time-series from several receivers, reversing the time direction of the signals, and simultaneously propagating the reversed signals from the receiver locations back into the medium, where they will eventually focus on the source location due to the constructive interference of the backpropagating wavefield from all individual receivers. Time reverse imaging has been used in non-destructive testing (Chakroun *et al.* 1995; Prada *et al.* 2002) and medical imagery (Fink *et al.* 2003; Fink 2010). Recent seismology applications of time reverse modelling have included imaging the sources of tremor from a hydrocarbon reservoir (Steiner *et al.* 2008), imaging the great Sumatra earthquake (Larmat *et al.* 2006), the scattering of regional surface waves (Stich *et al.* 2009) and location of synthetic tremor from a 2-D model of Mt Etna (Lokmer *et al.* 2009). Also Artman *et al.* (2010) have used different imaging techniques for time reverse location of a 2-D synthetic data set designed to locate tremor signals. Time reverse methods are strongly linked with adjoint methods (Tarantola 1988; Tromp *et al.* 2005; Fichtner *et al.* 2006). This can be explained through the invariance of seismic wave propagation to time reversal and is predicted by the symmetry of the wave equation operator. As yet, time reverse methods have not been applied to seismo-volcanic signals because it requires a high

density of stations to adequately capture the complex wavefield in such a complex medium and is computationally expensive. In the following we discuss the location method, test the location procedure with synthetic data and then describe the 2008 seismic data set. We locate two different families of events recorded during the 2008 effusive eruption on Mt Etna. Our time reversal locations are then compared with the locations from a cross-correlation method and with a full waveform moment tensor inversion method.

## 2 TIME REVERSAL

In the time reversal location method, the three component seismograms are flipped in time and used as seismic sources. In our case, we used all three component displacements from the seismograms as sources (input as single forces) located at the appropriate seismic station. The sources are then played back into a model using a seismic wave propagation code. The multiple sources generate seismic waves that propagate through the model where they interfere constructively and destructively and should focus on the original source location. Therefore, to locate the source origin, one has to image/select this convergence region from the 3-D wavefield at a time corresponding to maximum convergence. No assumptions are

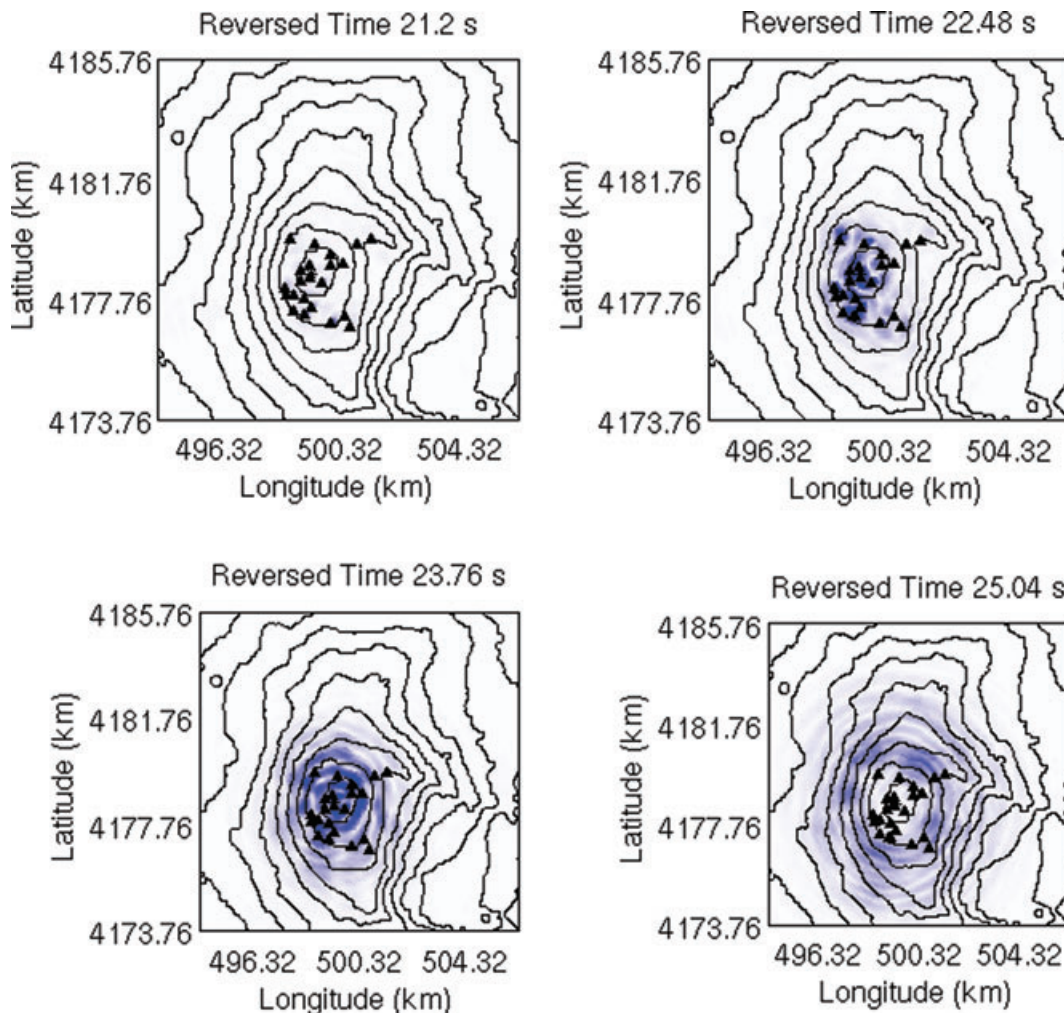


**Figure 1.** Numerical simulation of the time reversed wavefield converging on the source location for synthetic data generated by an explosive source located under the summit. The panels show the normalized displacement magnitude on the surface of the volcano. The triangles show the broad-band station distribution on Mt Etna, Italy during the 2008 June/July seismic deployment. See Supporting Information for an animation of this figure.

made and the wave propagation code is full waveform hence the only uncertainties in the location method, which should arise are from errors in the velocity model and poor wavefield sampling due to insufficient station coverage.

The energy current density vector (Larmat *et al.* 2009) is given by

$$J_i(\mathbf{x}, t) = -\left(\lambda \nabla \cdot \mathbf{u} + 2\mu \frac{\partial u_i}{\partial x_i}\right) \frac{\partial u_i}{\partial t} - \mu \sum_{i \neq j} \left(\frac{\partial u_j}{\partial x_i} + \frac{\partial u_i}{\partial x_j}\right) \frac{\partial u_j}{\partial t}, \quad (1)$$

where  $\lambda$  and  $\mu$  are the Lamé constants,  $\mathbf{u}$  is the displacement,  $\mathbf{x}$  the position and  $i$  and  $j$  are the spatial directions. The maximum of its magnitude is used to find the time at which the reversed wavefield focuses on the source location. At this time we output the imaging fields (displacement) for the source location. The source location is then chosen as the computational grid cell with the maximum displacement magnitude at this time. We did not use the energy current density to locate the events in space as we found that the displacement field gave a sharper image of the focus zone. We found that, since we are interested in shallow events, the large amplitude on the surface dominated the source location. This large amplitude arises as the sources are input on the surface and hence the wavefield amplitude is largest surrounding the sources. Therefore, to remove

the influence of the surface we damped out the surface amplitude by multiplying the displacement magnitude at all grid cells, at the time of maximum flux, by the distance from the cell to the nearest seismic station. It must be stressed that this was only done in the imaging stage to locate the source, not in the actual time reverse numerical simulation. Therefore, the effect of this damping is to remove the shallow regions surrounding the station positions as possible source locations. For deep sources as imaged in Lokmer *et al.* (2009) this step is unnecessary. We took this damping and imaging approach for time reverse imaging as (i) the 2-D location method used by Lokmer *et al.* (2009) for their synthetic tremor was not applicable in 3-D due to the computational cost of storing and imaging a 3-D wavefield; (ii) we wished to have an automated source location procedure removing human bias when selecting the source location visually; (iii) image analysis techniques proved difficult to implement because at different times during the simulation there were several different maximum displacement zones and using the maximum displacement in the search volume over all time did not work and (iv) as discussed earlier we wished to remove the bias of the large amplitude surface waves. This is a problem-specific approach that may not be viable for exceptionally shallow sources. Different imaging fields and time of convergence measures could have been used such as the divergence of the displacement, the curl

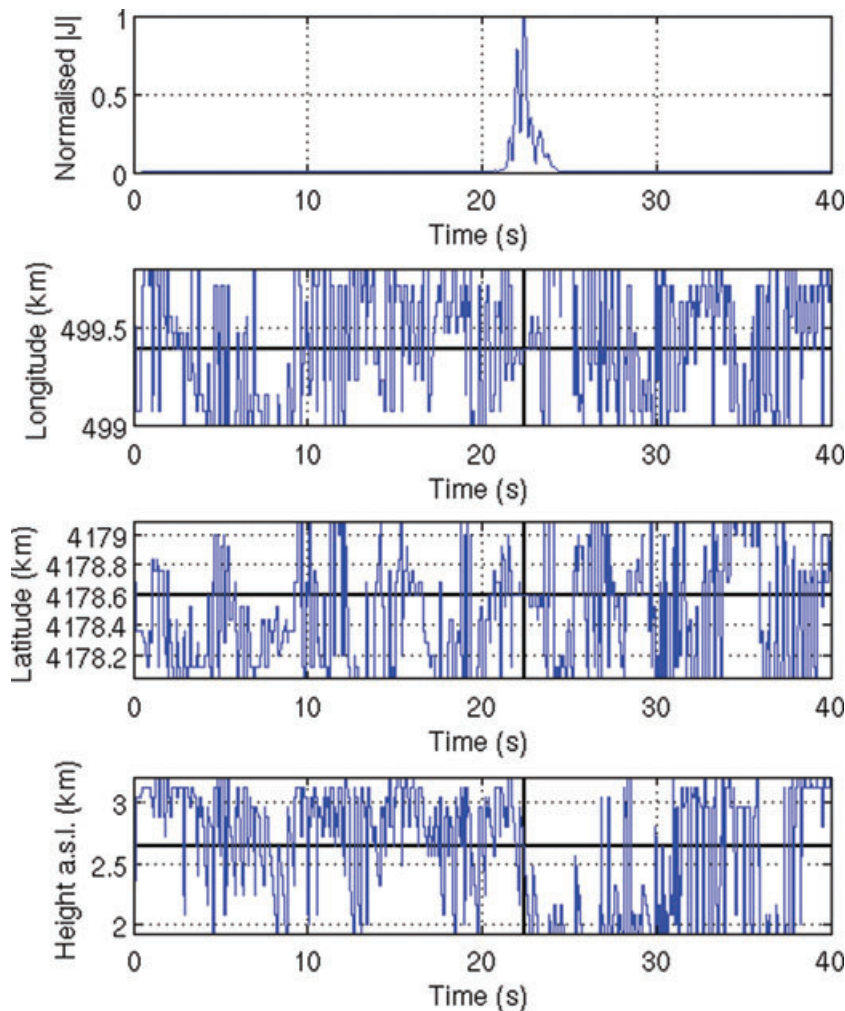


**Figure 2.** Upper panel: Maximum energy current density magnitude  $|J|$  in the computational volume as a function of time for the first synthetic test. Bottom panels: Spatial coordinates of the maximum displacement in the computational volume. The vertical line shows the time of maximum energy current density and gives the convergence time. The horizontal lines are the true source coordinates.

of the displacement, the divergence of the energy current density and/or the energy flux (Anderson *et al.* 2009a,b; Larmat *et al.* 2009). The energy current density magnitude and displacement field were used as the imaging fields for the source location as they gave the best results for the synthetic data. It should be noted that the energy current density magnitude can have a maximum value away from the true source location if there are high impedance contrasts. If this is the case, the divergence of the energy current density is a better imaging field. Larmat *et al.* (2009) demonstrated that imaging fields such as the divergence or the curl help with heterogeneous media. In our case, we assume a smooth/homogeneous velocity model as we are in the near field with low-frequency events. Before we used the time reversal method to locate the two families from the June/July data set we performed location tests on synthetic data.

### 3 SYNTHETIC TESTS

We use an elastic lattice method to model seismic wave propagation in a 3-D elastic medium including complex topography (O'Brien & Bean 2004). This method was used to generate the synthetic data sets and to propagate the time reversed seismic signals into our

model. Any full waveform wave propagation code would suffice. The computational costs involved in performing any 3-D full waveform simulation are high and require large memory and runtimes even using parallel architectures. The efficiency of the time reversed location method, from a computational point, will depend strongly on the wave propagation code used, the size of the model, the frequency of interest (higher frequencies require a smaller grid spacing hence larger resources), the hardware, the appropriate compilers and the optimization of all the components. We required three hour per time reverse simulation using a 64-processor parallel machine.

A digital elevation model of Mt Etna with a spatial resolution of 40 m was used in all simulations. We used a homogeneous velocity model with a  $P$ -wave set to  $2300 \text{ m s}^{-1}$  with a Poisson's ratio of 0.25. The model measures 30 km EW, 25 km NS and 12 km in the vertical direction with the synthetic station locations replicating the deployment of the 2008 experiment (Fig. 1). These values were chosen as they correspond to the velocity model used by De Barros *et al.* (2009) and Lokmer *et al.* (2010) to locate the same data set allowing us to compare results. We generated two different synthetic data sets for two different source mechanisms where the source time function used was a 1 Hz Ricker wavelet. The source mechanisms used were an isotropic source and a single vertical force located

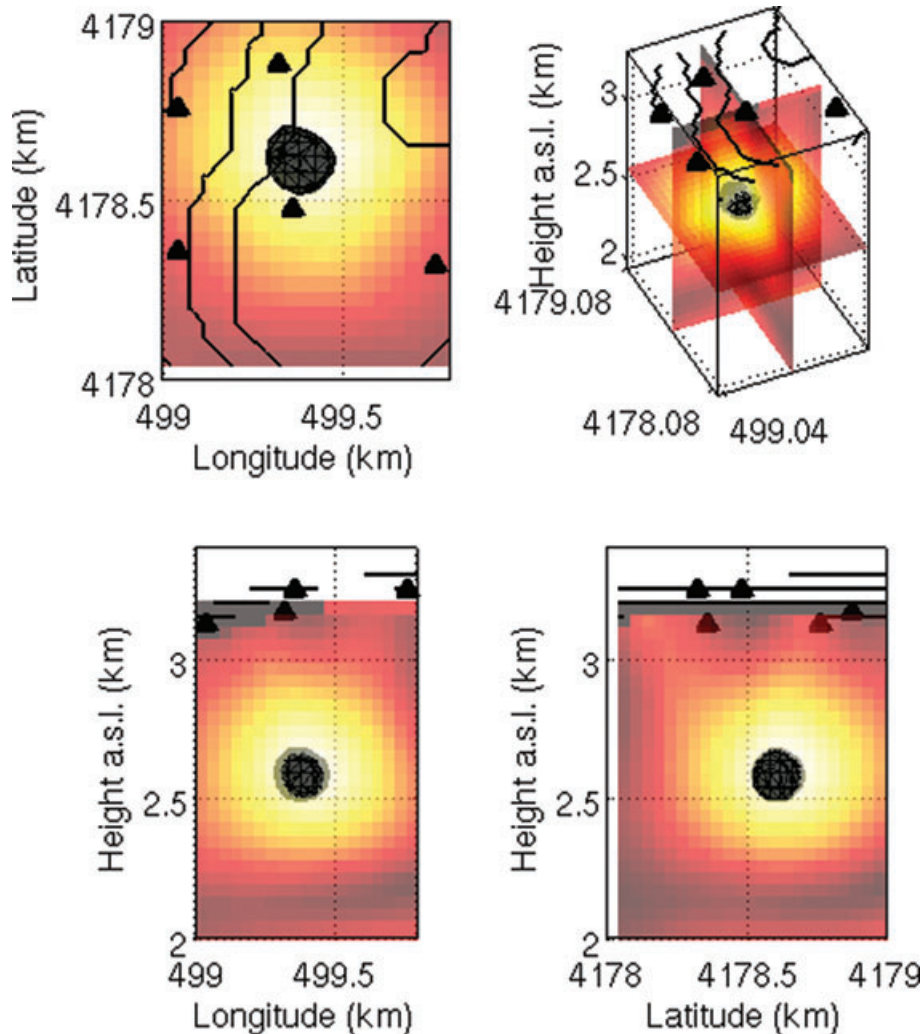


**Figure 3.** Normalized displacement field at the time of maximum energy current density in the grid for the first synthetic data set. The solid volume is the 95 per cent of the maximum amplitude contour and the source position is located within this region. The triangles are the positions of the nearest seismic stations. The black lines are elevation contours.

600 m below the surface. The synthetic data from these two simulations were then time reversed and used as single force sources. Fig. 1 shows the time reversed simulation of the displacement on the surface of the volcano at four different time steps for the isotropic synthetic data set. In the first snapshot, only distal stations input any energy into the model and as yet, the wavefield has not focused onto the source region. In the second snapshot the wavefield is starting to localize on the epicentre while in the final two snapshots the time reversed wavefield has focused on the epicentre and is now propagating outwards from it.

To retrieve the source location from the isotropic data set we calculated the maximum energy current density from all points inside the computational domain at every time step. We also tracked the spatial location of the maximum displacement magnitude multiplied by the distance to the nearest station. In our simulations we outputted the displacement at every time step that is unnecessary as only the displacement at the maximum energy flux is needed. For the sake of brevity we will call the maximum displacement magnitude multiplied by the distance to the nearest station the displacement unless otherwise specified. As discussed above this is to remove large amplitude on the surface. This results in four time-series for

the energy current density calculated using eq. (1) and the three components of the displacement (Fig. 2). The source origin time is given as the time of maximum energy current density, shown by the vertical line in Fig. 2. The true source coordinates are given by the horizontal lines in Fig. 2. A visual inspection of the 3-D displacement field shows several focus points throughout the simulation but as we approach in time, the maximum energy current density we see a large convergence of the wavefield on the source location, which then propagates outwards from this location. The sensitivity in selecting the correct time of convergence can be seen in Fig. 2. In both horizontal directions, the source position is stable over a few seconds around the time of convergence while a small change in time will lead to a larger error in the vertical position. The displacement at the time of maximum energy current density is shown in Fig. 3 where we can clearly see the displacement field centred on the source location in a spherical pattern. The solid contour in the Fig. 3 shows the contour of 95 per cent of the maximum amplitude with the true source position located inside this region. Fig. 4 shows a zoomed image of this figure with a transparent 95 per cent contour zone along with the source position and time reversal source location. The epicentre is fully recovered, however, the source depth

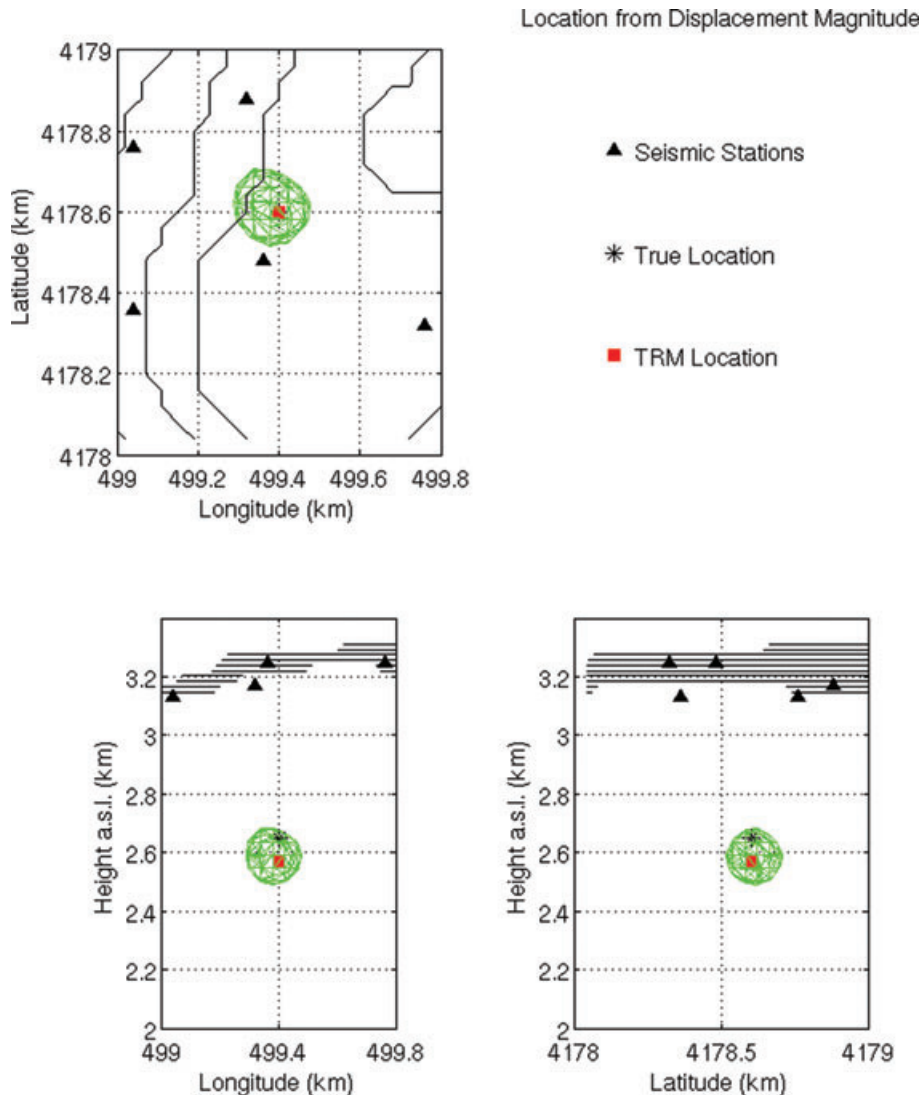


**Figure 4.** Time reverse source location and true location for the first synthetic data set (isotropic source). The hashed volume is the 95 per cent of the maximum displacement contour as shown in Fig. 3. The black lines are elevation contours.

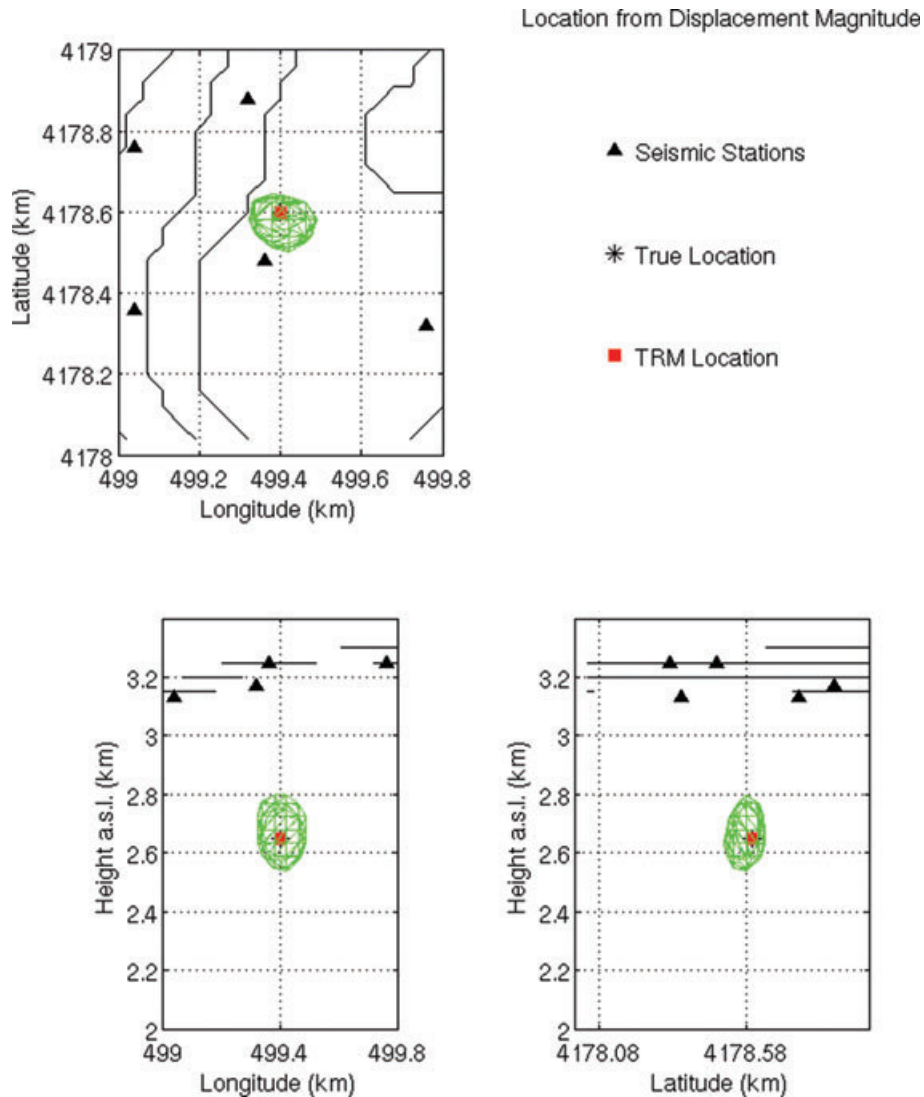


**Figure 5.** Time reverse source location and true location for the second synthetic data set (vertical force source). The hashed volume is the 95 per cent of the maximum displacement contour. In this test the source is non-isotropic giving rise to the oblong source region. The black lines are elevation contours.

is overestimated by 80 m but lies within the contoured region. A vertical single force was used to generate the second synthetic data set as  $S$  waves are generated leading to a more complex radiation pattern. We followed the same procedure as above but in this case we have exactly recovered the source position (Fig. 5). It can be seen from Figs 3 and 4 that the source zone is spherical and differs from the oblong source zone in Fig. 5. Therefore, we investigated if we can recover any information about the source mechanism from the displacement field. We also calculated the divergence and curl of the displacement field along with the strain tensor and stress tensor. None of these calculations provided reliable source mechanisms as was observed in the 2-D tests of Lokmer *et al.* (2009). We attribute this to a distortion of the radiation pattern by the surface. Scattering from the surface distorts the wavefield and since we are sparsely sampling it we cannot fully capture the original radiation pattern, hence, we cannot image any information about the source mechanism. Also, the difficulty in interpreting the complex 3-D wavefield combined with the irregular station distribution will negate our ability in this case to extract information about the source mechanism. Along with this, the recording stations are in the near field so the  $P$  waves,  $S$  waves, surface waves and scattered waves are all inter-

twined making it difficult to interpret the complex 3-D wavefield with a relatively small array aperture. As with all location methods, it is sensitive to the velocity model. A detailed discussion of the effect of changing the velocity model is given in Lokmer *et al.* (2009).

#### 4 DATA

From 2008 June 18 to 2008 July 3, a total of 50 stations with three component broad-band sensors were deployed on Mt Etna volcano (Fig. 1). This included 16 permanent stations from INGV, Italy and 34 temporary stations from University College Dublin (Ireland), Universite de Savoie (France) and INGV (Italy). To extract the LP events, a STA/LTA method on the bandpass filtered data (0.2–1.5 Hz) was used which gave approximately 500 events (De Barros *et al.* 2009). These events were then classified using a cross-correlation analysis between all pairs of signals (Saccorotti *et al.* 2007) and two different families were obtained with a similar number of events (Fig. 6). Both families were filtered in the range 0.2–0.8 Hz. The first family consists of 63 events and the

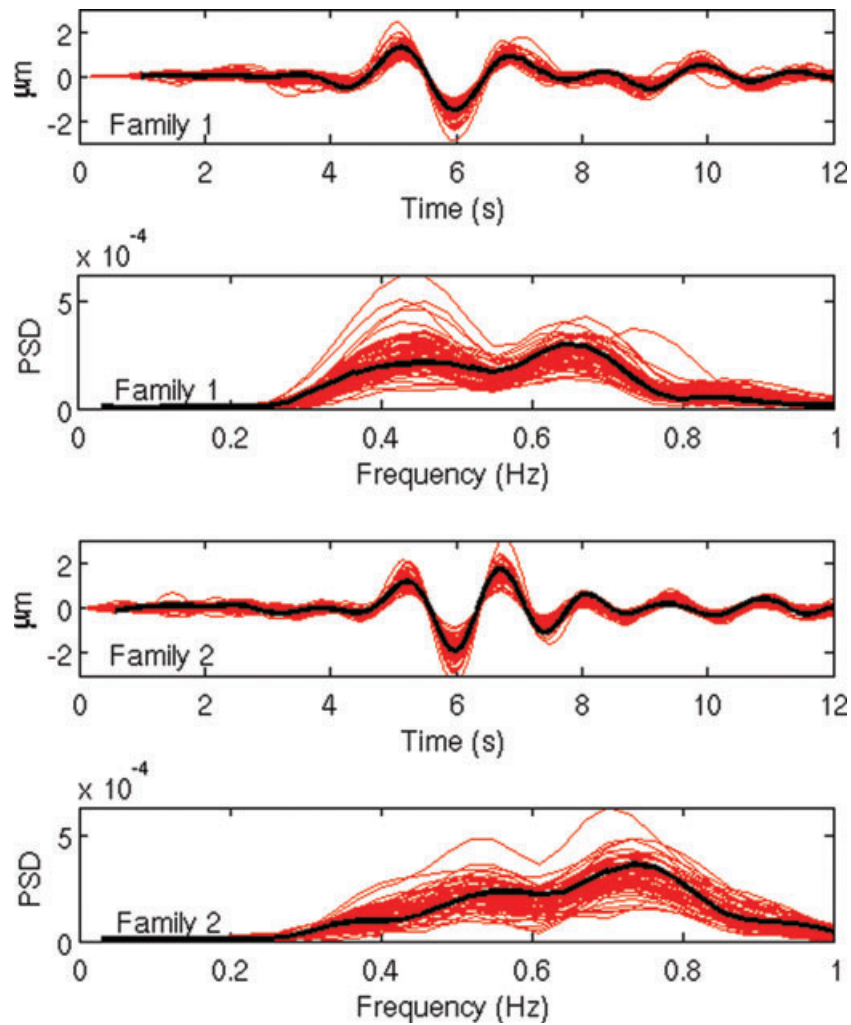


**Figure 6.** Waveform and spectral content of the vertical component of the LP families recorded at station ECPN during the 2008 seismic deployment filtered between 0.2 Hz and 0.8 Hz. The top panels are for family 1 and the bottom two are for family 2. The heavy line is the stack of the family. The waveform consists of *P* waves, *S* waves, surface waves and scattered waves intertwined. We backpropagate the entire signal shown.

second family of 66 events. In the time reverse method we used the full waveform (12 s). The LP signals shown are pulse-like and not resonating signals which reduces the simulation time. Only the near-field stations (Fig. 1) were considered as the amplitude of the signals was low and the signal-to-noise ratio for the far-field stations was very poor (De Barros *et al.* 2009). The waveform similarity within each family would suggest a spatially close source with a similar mechanism, while the source position and/or the mechanism are almost certainly different between the two families.

## 5 RESULTS

Using the procedure outlined above, we located all the events in both families. For each event we used a minimum of 13 stations located close to the source from the 23 possible stations (Fig. 1). An animation of this figure is included as Supporting Information. This was done to compare with the location results from De Barros *et al.* (2009) and Lokmer *et al.* (2010) who used 23 stations from the possible 50. The effect of the more distal stations is expected to be negligible as the initial amplitudes are small relative to the near-field stations and the amplitudes further decrease due to geometric

spreading before they reach the focus zone. Also, in our case, the signal-to-noise ratio for the far-field stations was very poor.

Fig. 7 shows the location of the events in family 1 with several events located in the same position. We have also plotted the location results from De Barros *et al.* (2009) and Lokmer *et al.* (2010). The source positions are clustered together using the time reversal method and moment tensor method. We find that the moment tensor and time reversal methods give approximately the same result with a difference of approximately 200 m in depth and 200 m in longitude. The similarity between the two is not surprising since time reversal imaging gives an approximate solution to source inversion techniques (Kawakatsu and Montagner 2008). The small difference, relative to the wavelength, in the source locations could be attributed to (i) noise in the data interfering with the inversion procedure and the time reversal method, (ii) scaling the displacement to remove the surface amplitudes lowering the time reverse location, though this effect is not seen in the synthetics or (iii) a trade-off between the source mechanism and source location in the inversion shifting the source, that is, finding an artificially lower misfit value by exploring a large parameter space. The cross-correlation locations are more elongated than the moment tensor and time reverse locations. The method assumes the source is isotropic and that the far-field

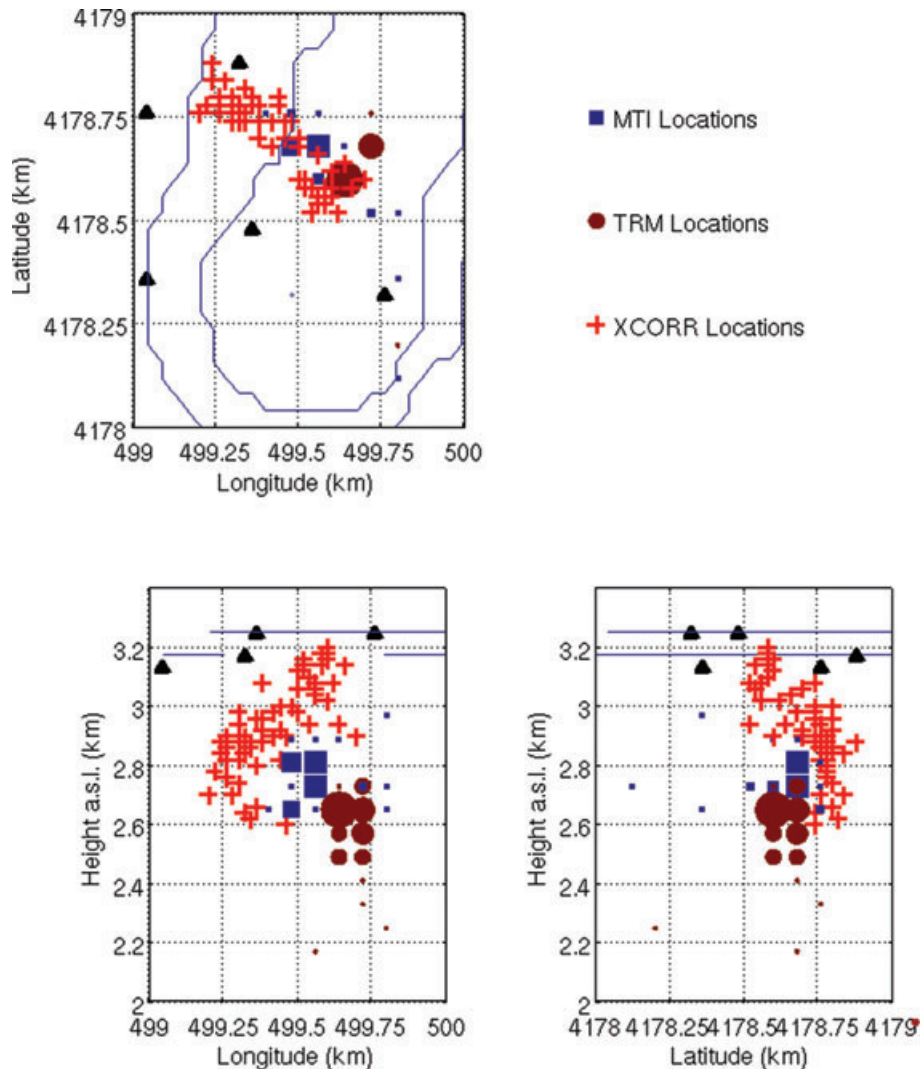


**Figure 7.** Comparison of the time reversal locations (circles) with a full waveform moment tensor inversion location (squares) and with a cross-correlation location method (crosses) for family 1. The size of the circle/square indicates the number of LP events located at that spot, largest circle/square, 25 events, smallest circle 1 event. The triangles represent seismic stations.

term dominates the wavefield, which combined with the noise in the data, possibly generates the large scattering. There is no way of determining which of the methods, if any, gives the most accurate source positions, however, considering the wavelength and the size of the volcano, a similar source region is recovered. Fig. 8 shows the results for family 2. Compared with the other methods, the time reversal method gives a more localized source region but with a deeper source. The difference in depth between the time reversal and other two methods could be related to the damping of the shallow structure. When we remove the damping we locate these events on the surface at the same epicentre. Family 2 has been shown to have a source mechanism that consists of more than 80 per cent isotropic component (Lokmer *et al.* 2009) which may explain why the cross-correlation method is more similar to the moment tensor and time reversal locations than observed in family 1. The summed displacement field at the time of maximum energy density from all the events in family 1 and family 2 is shown in Fig. 9 along with the 95 per cent contour of the maximum amplitude. The stacked displacement fields are similar to the individual events. This volume encompasses the region of maximum seismic radiation, and should not be considered a geological structure though we cannot rule this

possibility out. It can be clearly seen that the displacement field for family 1 is far more dispersed than in family 2. The focus region of the time reversed wavefield for family 1 resembles a cylindrical structure dipping  $\sim 60^\circ$  west. This region could be a consequence of (i) not fully capturing and reversing the entire wavefield resulting in a smearing of the time reversed wavefield; (ii) the reconstruction of a complex radiation pattern [the source mechanism of family 1 consists of 60 per cent isotropic and 40 per cent CLVD, (Lokmer *et al.* 2010)]; (iii) an inadequate velocity model or (iv) seismicity generated on a geological structure. Family 2 is more localized and resembles the time reversed wavefield from the isotropic synthetic test. This would indicate a common source position with a high isotropic component in the source.

## 6 CONCLUSIONS

We have examined the possibility of using 3-D time reversal of LP seismograms to image the location of these events on Mt Etna. In our synthetic tests satisfactory images of the known source locations have been recovered. We then located two LP families recorded during the 2008 effusive eruption. Family 1 encompasses a

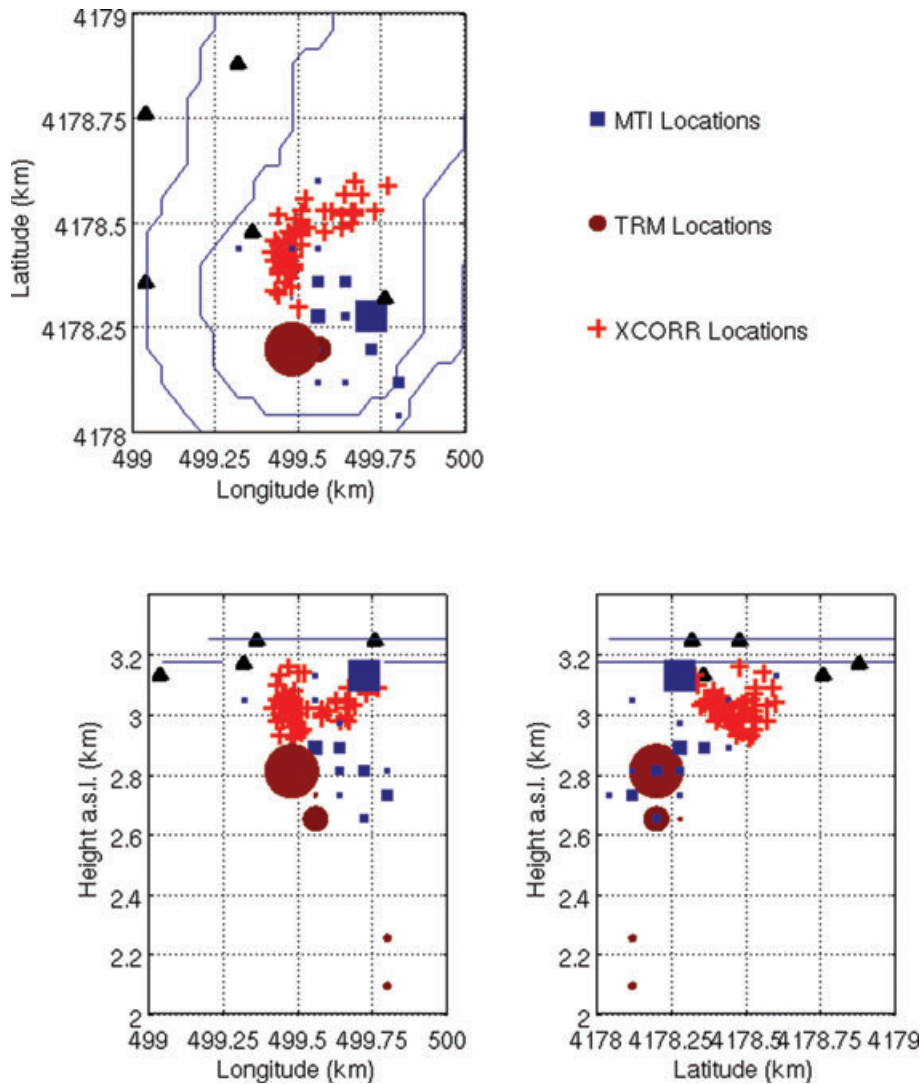


**Figure 8.** Comparison of the time reversal locations (circles) with a full waveform moment tensor inversion location (squares) and with a cross-correlation location method (crosses) for family 2. The size of the circle/square indicates the number of LP events located at that spot, largest circle/square, 49 events, smallest circle 1 event. The triangles represent the seismic station locations.

cylindrical-like region dipping  $60^\circ$  west whereas family 2 is located in a shallower more localized region. These source regions are consistent with the locations of both families using a cross-correlation and moment tensor source inversion technique. The time reverse locations are more compatible with the moment inversion method for family 1. The time reverse imaging technique was not able to provide any reliable information about the possible source mechanism generating the LP events. Given the consistent locations with two other methods, time reverse imaging offers an alternative approach to locating LP events in volcanic regions. A great advantage of this method for locating emergent LP volcanic events over the more traditional techniques, is that the method is not affected by (i) the scattering of the wavefield on topography, (ii) the intertwining of  $P$  and  $S$  waves and/or (iii) the strong variations of the distance-dependent spectrum of the near-field term as all these effects are included in the numerical simulations. The similarity between the time reverse location and moment tensor inversion grid search technique allows us to fix the source location using one single time reverse simulation. This location can then be used to perform a moment tensor inversion. This once off inversion considerably reduces

the calculations necessary to perform a grid search full waveform inversion. The application of the technique still requires further tests to explore the effect of the station distribution, number of stations, incorrect velocity model and correcting for a sparse sampling of the wavefield by weighting the station amplitudes according to the surface area they cover. Also, the effect of correcting amplitudes to account for the irregular spatial sampling of the wavefield should be explored (Larmat *et al.* 2009). This can be readily achieved by calculating the site amplification factors determined from regional earthquakes. This procedure is routinely applied when using the amplitude decay method to locate volcano seismic signals, (Battaglia & Aki 2003). However, our data set did not contain enough regional earthquakes to perform such a correction. The further tests should also examine the possibility of using the different imaging fields discussed in Section 2 to locate the source and possibly provide some information about the source mechanism though this seems unlikely for shallow events with long wavelengths. In summary, the 3-D time reversed source image can reveal the location and extent of the seismic source region avoiding some of the *a priori* assumptions used in alternative location techniques.

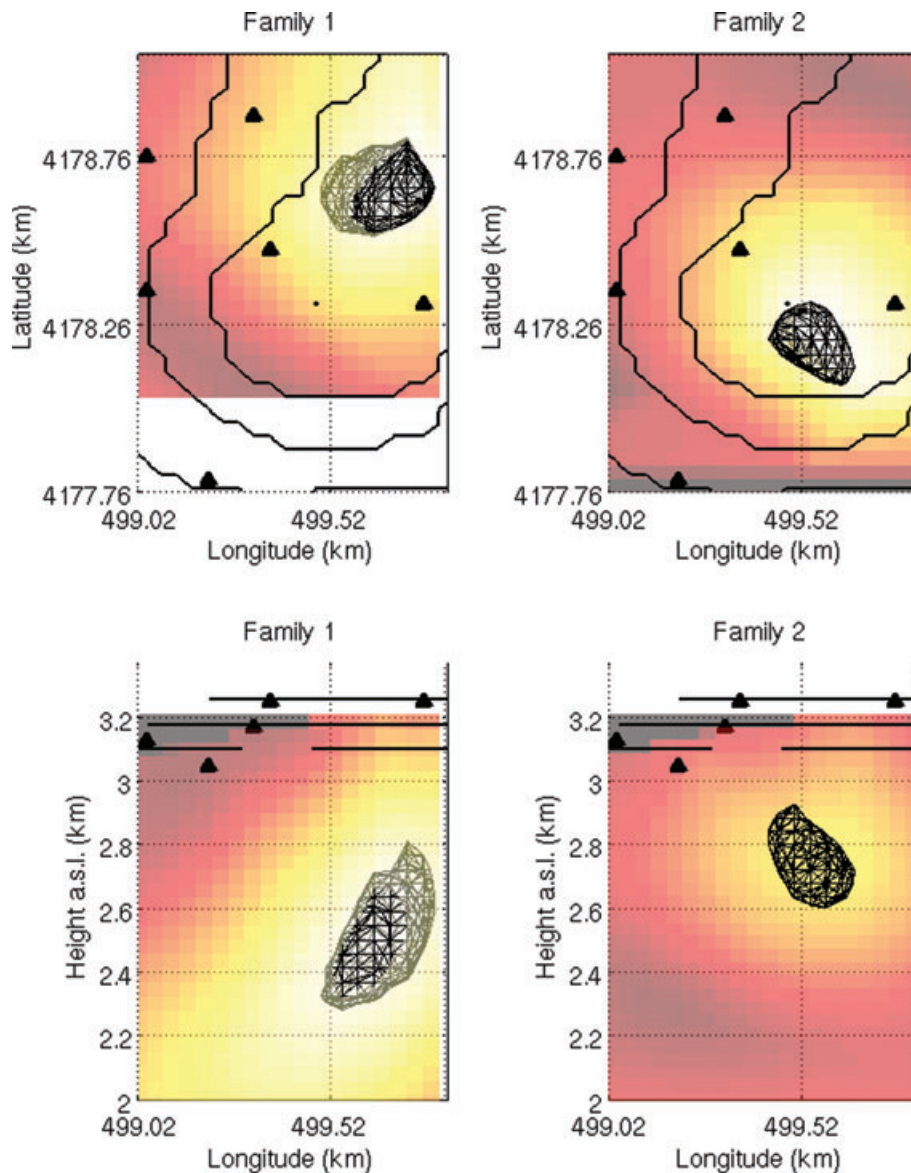


**Figure 9.** Total normalized displacement field for all events in family 1 (left-hand panels) and family 2 (right-hand panels), (bright being 1 and dark 0). The top panels show the map view and the bottom panels show the EW cross-section. The hashed volume is the 95 per cent of the maximum amplitude contour and is the region for which there is maximum likelihood of source location. The triangles show the position of the nearest seismic stations.

## ACKNOWLEDGMENTS

The authors wish to acknowledge that this work was carried out in part under the Department of Communications, Energy and Natural Resources under the National Geoscience Programme 2007–2013 and the SFI RFP 2007 awards. The SFI/HEA Irish Centre for High-End Computing (ICHEC) is acknowledged for the provision of computational facilities and support. The comments and suggestions from Alex Goetz, an anonymous reviewer and the Associate Editor greatly improved the original manuscript.

## REFERENCES

- Almendros, J., Chouet, B. & Dawson, P., 2001. Spatial extent of a hydrothermal system at Kilauea Volcano, Hawaii, *J. geophys. Res.*, **106**(B7), 13 581–13 597.
- Anderson, B.E., Guyer, R.A. & Ulrich, T.J., 2009a. Time reversal of continuous-wave, steady-state signals in elastic media, *Appl. Phys. Lett.*, **94**, 111908, doi:10.1063/1.3097811.
- Anderson, B.E., Guyer, R.A., Ulrich, T.J., Le Bas, P.-Y., Larmat, C., Griffa, M. & Johnson, P.A., 2009b. Energy current imaging method for time reversal in elastic media, *Appl. Phys. Lett.*, **95**, 021907, doi:10.1063/1.3180811.
- Artman, B., Podladtchikov, I. & Witten, B., 2010. Source location using time-reverse imaging, *Geophys. Prospect.*, **58**, 861–873.
- Battaglia, J. & Aki, K., 2003. Location of seismic events and eruptive fissures on the Piton de la Fournaise volcano using seismic amplitudes, *J. geophys. Res.*, **108**(B8), 2364, doi:10.1029/2002JB002193.
- Chakroun, N., Fink, M. & Wu, F., 1995. Time reversal processing in ultrasonic nondestructive testing, *IEEE Trans. Ultrason. Ferroelectr. Freq. Control*, **42**(6), 1087–1098.
- Chouet, B., 2003. Volcano seismology, *Pure appl. Geophys.*, **169**, 739–788.
- De Barros, L., Bean, C.J., Lokmer, I., Saccorotti, G., Zuccarello, L., O'Brien, G.S., Metaxian, J.P. and Patane, D., 2009. Source geometry

- from exceptionally high resolution Long Period event observations at Mt Etna during the 2008 eruption, *Geophys. Res. Lett.*, **36**, doi:10.1029/2009GL041273.
- Di Lieto, B., Saccorotti, G., Zuccarello, L., La Rocca, M. & Scarpa, R., 2007. Continuous tracking of volcanic tremor at Mount Etna, Italy, *Geophys. J. Int.*, **169**, 699–705.
- Fichtner, A., Bunge, H.P. & Igel, H., 2006. The adjoint method in seismology. I. Theory, *Phys. Earth planet. Inter.*, **157**, 86–104.
- Fink, M., 2010. Multiwave imaging and superresolution, *Phys. Today*, (63), 28–33.
- Fink, M., Montaldo, G. and Tanter, M., 2003. Time-reversal acoustics in biomedical engineering, *Annu. Rev. Biomed. Eng.*, **5**, 465–497.
- Kawakatsu, H & Montagner, J-P., 2008. Time-reversal seismic-source imaging and moment-tensor inversion, *Geophys. J. Int.*, **175**, 686–688, doi:10.1111/j.1365-246X.2008.03926.x
- Kumagai, H. et al. 2010. Broadband seismic monitoring of active volcanoes using deterministic and stochastic approaches, *J. geophys. Res.*, **115**, B08303, doi:10.1029/2009JB006889.
- Larmat, C., Montagner, J-P., Fink, M., Capdeville, Y., Tourin, A. & Clévé dé, E., 2006. Time-reversal imaging of seismic sources and application to the great Sumatra earthquake, *Geophys. Res. Lett.*, **33**, L19312, doi:10.1029/2006GL026336.
- Larmat, C.S., Guyer, R.A. Johnson, P.A., 2009. Tremor source location using time reversal: selecting the appropriate imaging field, *Geophys. Res. Lett.*, **36**, L22304, doi:10.1029/2009GL040099.
- Lokmer, I., Bean, C.J., Saccorotti, G. & Patané, D., 2007. Moment-tensor inversion of LP events recorded on Etna in 2004 using constraints obtained from wave simulation tests, *Geophys. Res. Lett.*, **34**, L22316, doi:10.1029/2007GL031902.
- Lokmer, I., O'Brien, G.S., Stich, D. & Bean, C.J., 2009. Time reversal imaging of synthetic volcanic tremor sources, *Geophys. Res. Lett.*, **36**, L12308, doi:10.1029/2009GL038178.
- Lokmer, I., O'Brien, G.S., De Barros, L. and Bean, C. 2010. High-resolution spatio-temporal source inversion of a long-period (LP) sequence recorded by a dense broadband network, *Geophys. Res. Abstr.*, **12**, EGU2010-13706.
- McNutt, S., 2005. Volcanic Seismology, *Annu. Rev. Earth planet. Sci.*, **32**, 461–491.
- Métaxian, J. Ph. & Lesage, P., 2002. Locating sources of volcanic tremor and emergent events by seismic triangulation: application to Arenal volcano, Costa Rica, *J. geophys. Res.*, **107**(B10), 2243, *ECV* **10**, 1–18.
- Nakano, M. & Kumagai, H., 2005. Waveform inversion of volcano-seismic signals assuming possible source geometries, *Geophys. Res. Lett.*, **32**(12), L12302, doi:10.1029/2005GL022666.
- O'Brien, G.S. & Bean, C.J., 2004. A 3D discrete numerical elastic lattice method for seismic wave propagation in heterogeneous media with topography, *Geophys. Res. Lett.*, **31**(14), L14608, doi:10.1029/2004GL020069.
- Ohminato, T., Chouet, B.A., Dawson, P. & Kedar, S., 1998. Waveform inversion of very long period impulsive signals associated with magmatic injection beneath Kilauea Volcano, Hawaii, *J. geophys. Res.*, **103**, 23839–23862.
- Prada, C., Kerbrat, E., Cassereau, D. & Fink, M., 2002. Time reversal techniques in ultrasonic nondestructive testing of scattering media, *Inverse Probl.*, **18**, 1761–1773, doi:10.1088/0266-5611/18/6/320.
- Saccorotti, G., Lokmer, I., Bean, C., Grazia, G.D. & Patane, D., 2007. Analysis of sustained long-period activity at Etna Volcano, Italy, *J. Volc. Geotherm. Res.*, **160**, 340–354.
- Steiner, B., Saenger, E.H. & Schmalholz, S.M., 2008. Time reverse modelling of low-frequency microtremors: application to hydrocarbon reservoir localization, *Geophys. Res. Lett.*, **35**, L03307, doi:10.1029/2007GL032097.
- Stich, D., Danecek, P., Morelli, A. & Tromp, J., 2009. Imaging lateral heterogeneity in the northern Apennines from time reversal of reflected surface waves, *Geophys. J. Int.*, **177**, 543–554.
- Tarantola, A., 1988. Theoretical background for the inversion of seismic waveforms, including elasticity and attenuation, *Pure appl. Geophys.*, **128**, 365–399.
- Tromp, J., Tape, C. & Liu, Q., 2005. Seismic tomography, adjoint methods, time reversal and banana-doughnuts kernels, *Geophys. J. Int.*, **160**, 195–216.

## SUPPORTING INFORMATION

Additional Supporting Information may be found in the online version of this article:

**Figure S1.** An animated numerical simulation of the time reversed wavefield converging on the source location for synthetic data generated by an explosive source located under the summit. The panels show the normalized displacement magnitude on the surface of the volcano. The triangles show the broad-band station distribution on Mt Etna, Italy during the 2008 June/July seismic deployment.

Please note: Wiley-Blackwell are not responsible for the content or functionality of any supporting materials supplied by the authors. Any queries (other than missing material) should be directed to the corresponding author for the article.